Secure UAV-to-Vehicle Communications

Tingting Li, Jia Ye, *Student Member, IEEE*, Jibo Dai, Hongjiang Lei, *Senior Member, IEEE*, Weiwei Yang, Gaofeng Pan, *Senior Member, IEEE*, Yunfei Chen, *Senior Member, IEEE*

***Abstract*—Unmanned aerial vehicles (UAVs) communications have been widely exploited in our daily life, which leads to rising concerns about the security issue. This work investigates the secrecy performance of a UAV-to-vehicle (UAV-2-V) communication system, where the information delivered over both downlink and uplink between a UAV (S) acting as a temporary aerial base-station and a legitimate vehicle (D) moving along a road is overheard by an eavesdropping vehicle (E) on the same road. The location of S is assumed to be uniformly distributed in the sky, while the locations of D and E are uniformly distributed on the highway. The statistical characteristics, including the cumulative distribution function and probability density function of the received signal-to-noise ratio over both downlink and uplink, are characterized respectively. Closed-form expressions for the approximate and asymptotic secrecy outage probability (SOP) of the downlink experiencing Rician fading channels have been derived accordingly. Moreover, the secrecy outage performance of the uplink is investigated by deriving the closed-form expression of the exact and asymptotic SOP in two cases: the eavesdropping channel suffers Rician and Weibull fading, respectively. Finally, Monte-Carlo simulations are shown to verify our proposed analytical models.**

***Index Terms*—Secrecy outage performance, secure UAV-to-vehicle communications, stochastic geometry, unmanned aerial vehicles.**

I. Introduction

Benefiting from their inherent attributes such as flexibility, easy deployment, low maintenance cost, and controllable mobility, unmanned aerial vehicles (UAVs) have become one of the most attractive candidates to satisfy the 5G and beyond communications networks [1], [2]. UAVs are also widely applied from the military domain to the civilian and commercial domains [3], playing a critical role in wireless communication systems to support emergency communications, data collection, surveillance, and environmental monitoring. In these applications, the reliability, throughput, and coverage can be greatly enhanced by deploying UAVs as relays to forward the information from a source to a destination [4]–[6], or as aerial base stations to disseminate data to ground terminals [7]–[11]. In particular, UAV-based flying stations can overcome the drawbacks of the static ground base station. Moreover, ground users can avoid staying in a deep fade forever and enjoy a significant reduction in average fade duration by adopting aerial base station [12]. Many researchers have worked on this topic from the perspective of placement planning, trajectory design, and performance analysis, such as [13] and [14]. Authors in [13] proposed two stochastic trajectory processes, namely, spiral and oval processes, and analytically demonstrated that the same coverage as the static case was achievable and average fade duration was enhanced. A simple mixed mobility model for the UAV movement process in three-dimensional (3D) space was proposed in [14], and the coverage probability was analyzed of a reference uesr equipment in a finite network with multiple UAVs under the uniform and closest UAV association policies.

As far as the system performance is concerned, the secrecy performance of UAV communication systems is of utmost concern due to the openness of the wireless propagation environment. The line-of-sight (LOS) links between UAV and ground devices are more challenging to protect and are more susceptible to terrestrial eavesdroppers. Since the traditional cryptographic-based methods are not the optimal method for high-mobility UAVs, physical layer security has been broadly considered as a key complementary approach for various kinds of secure wireless communications [15]–[17]. This probabilistic method can characterize the likelihood of a wireless network achieving a secrecy rate by considering the channel randomness [18]. For example, the closed-form approximation of the intercept probability of a UAV-assisted relaying communication system was studied in [19], [20], while the exact expression of the secrecy outage probability (SOP) between the ground device and UAV has been investigated in [21], [22]. The trajectories and transmit power of the UAV communication systems with the aid of a UAV jammer were optimized in [23] to maximize the minimum average secrecy rate over all the users and an alternating iterative algorithm utilized the successive convex approximation technique was proposed. UAVs were utilized as relays was investigated in [24] , and the secrecy performance of the hybrid satellite-terrestrial networks with different relay selection strategies was studied.

Manuscript received Sep. 28, 2020; revised Feb. 9, 2021; accepted Apr. 11, 2021. This research was supported by the NSF of China under Grant 61971080 and 61771487, the Open Fund of the Shaanxi Key Laboratory of Information Communication Network and Security under Grant ICNS201807. The associate editor coordinating the review of this paper and approving it for publication was N. Lee. (Corresponding author: Gaofeng Pan)

T. Li is with the School of Mathematics and Statistics, Southwest University, Chongqing, 400715, China.

J. Ye is with Computer, Electrical and Mathematical Sciences and Engineering Division, King Abdullah University of Science and Technology (KAUST), Thuwal 23955-6900, Saudi Arabia.

J. Dai is with National Key Laboratory of Science and Technology on Aerospace Intelligence Control, Beijing 100854, China, and he is also with Beijing Aerospace Automatic Control Institute, Beijing 100854, China.

H. Lei is with Chongqing Key Laboratory of Ubiquitous Sensing and Networking, Chongqing University of Posts and Telecommunications, Chongqing 400065, China, and also with Shaanxi Key Laboratory of Information Communication Network and Security, Xi'an University of Posts and Telecommunications, Xi'an 710121, China.

W. Yang is with Army Engineering University of PLA, Nanjing 210007, China.

G. Pan is with the School of Cyberspace Science and Technology, Beijing Institute of Technology, Beijing 100081, China.

Y. Chen is with the School of Engineering, University of Warwick, Coventry, CV4 7AL, U.K.

Most of these works only considered UAVs' mobility while ignoring the location randomness and mobility of ground users and eavesdroppers. The authors in [22] investigated the secrecy performance of a legitimate ground link in the presence of friendly jamming and UAV eavesdroppers following a uniform binomial point process. The SOP minimization problem was studied in [25] subject to the mobility constraint and location constraint of a multi-antenna UAV-enabled mobile relaying system in the presence of a multi-antenna eavesdropper. UAVs with fully controllable mobility were adopted in [26] to facilitate secure communication by adaptively adjusting their locations over time and cooperative jamming. The outage performance of UAV communications was characterized while considering the mobility of ground users [27]. Assuming that users are uniformly distributed, the authors of [28] derived the analytical expressions for the outage probability and the ergodic rate of non-orthogonal multiple access (NOMA) enhanced UAV networks.

However, these afore-mentioned works do not consider the secrecy problem. So far, only a few works were to presented to analyze the secrecy performance while considering the randomness of ground users' locations. Ref. [29] characterized the physical layer security of the link between the ground source and UAV, while a random number of eavesdroppers are randomly positioned around the ground source. The authors in [30] investigated the security of multiple UAV-assisted communication, where eavesdroppers on the ground and UAVs in the air follow homogeneous Poisson point processes. Considering that users and eavesdroppers follow independent homogeneous Poisson point processes, the downlink UAV networks' security, reliability, and energy coverage performance under NOMA and orthogonal multiple access schemes have been studied in [31]. The authors of [10] investigated the secrecy outage performance of a UAV-to-ground communication system with a linear trajectory, while an eavesdropping UAV tried to overhear the delivered information. The position randomness of the UAV transmitter and the UAV eavesdropper is assumed for the uplink transmission, while the position randomness of the ground user and the UAV eavesdropper is assumed for the downlink transmission. None of these works has evaluated the security performance considering all the location randomness of UAV, the legitimate user, and the eavesdropper, which motivates us to mitigate this gap.

Nowadays, users expect to gain reliable and low latency service all the time, even when they are in the vehicles moving on the highway/street. Existing researches showed that smart cities could not be achieved without a reliable and efficient transportation system [32]. Among these scenarios, the use of UAVs is receiving significant interest. For instance, UAVs can fly over vehicles on a highway to monitor and report possible traffic violations. The mobility of UAVs enables it to easily establish the connection with ground moving vehicles that experience difficulties in communicating with each other due to obstacles including high-rise buildings. Overall, UAVs can provide an efficient means not only to provide road users with efficient information on traffic but also to tackle the communication challenges faced by vehicles on the ground. Various researches have been carried out to optimize the connection performance between UAVs and vehicles by designing the altitude, position, and trajectory [33], [34], while little attention is put on the secrecy performance for the UAV-to-Vehicles (UAV-2-V) system.

In summary, no works have been presented to study the secure information delivery in UAV-2-V systems. However, the investigation of the secure information transmission in UAV-2-V systems is necessary to understand the influence of system factors. In this work, a UAV-2-V system is considered, where a UAV (S) acting as a temporary aerial station tries to deliver/collect information to/from a legitimate vehicle (D). The communication process between S and D is intercepted by an eavesdropping vehicle E. Specifically, S is uniformly distributed in the sky, D and E are uniformly distributed on the highway. The tools from stochastic geometry theory are employed to investigate the impact of the randomness of S in 3-dimensional (3D) space, and that of D and E on the road to the downlink and uplink secrecy outage performance.

The main contributions of this work are summarized as follows:

1) We characterize the statistical characteristics including cumulative distribution functions (CDF) and probability density function (PDF) of the received signal-to-noise ratio (SNR) at D, E over the downlink, at S over the uplink, and at E from D under different channel propagation, respectively.

2) We derive the approximate and asymptotic analytical expressions for the SOP over the uplink while assuming that all channels experience Rician fading.

3) We derive closed-form analytical expressions for the exact and asymptotic SOP over the downlink while two different kinds of channel fading between D and E (namely, Rician and Weibull fading) are respectively considered.

4) We systematically investigate the impacts of the radius of the coverage space of S, and the height of the UAV on the secrecy outage performance of the considered UAV-2-V system.

II. System Model

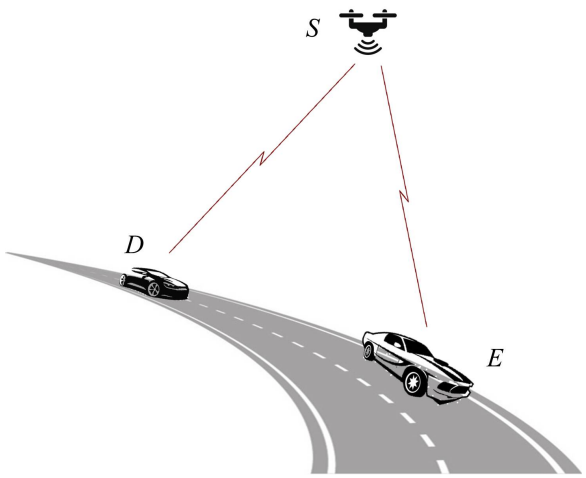

Fig. 1: UAV-2-V communication scenarios

In this work, we consider a UAV-2-V communication system

shown in Fig. 1 [1], in which a UAV (S) plays as a temporary aerial base-station to deliver/collect information to/from a legitimate vehicle (D), while an eavesdropping vehicle (E) moves on the same linear road with D and tries to overhear the information exchange between S and D. Moreover, it is assumed that $S-D$ and $S-E$ links suffer from independent and identically distributed Rician fading.

One of the advantages of UAV is the flexibility for quick deployment. In this work, UAV is used to substitute for the on-ground base-stations that are out of service due to some emergency (e.g., earthquake) or fulfill the blind coverage area without any terrestrial infrastructure. Then, we assume that the location of S is uniformly distributed in the sky. Without loss of generality, in this work, it is also assumed that D and E are uniformly distributed on the highway, which is modelled as a straight line here to facilitate the following analysis.

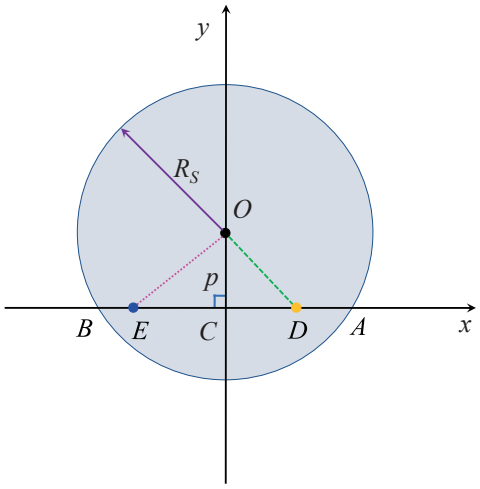

Fig. 2: 2-dimensional model for UAV-2-V link.

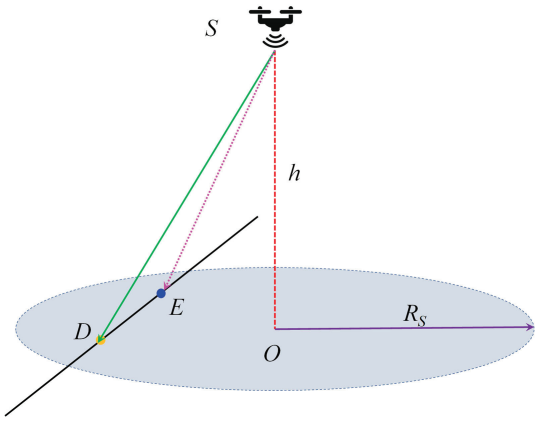

Fig. 3: 3D model for UAV-2-V link.

[1] There are some practical application scenarios for the considered model presented in Fig. 1, e.g., during patrols or pursuit missions, UAVs are usually used to aid the police on the road/highway to set up communications with the command centra. However, due to the openness of the application scenarios, eavesdropping cannot be totally prohibited. Moreover, for simplification purposes, in this work we consider a simplest scenario depicted in Fig. 1 to propose our analytical method, which can serve as a useful reference to investigate the performance of other similar UAV communication systems.

As depicted in Fig. 2, the coverage area of S on the ground is a circle with radius R_S and centre O (in other words, the projection of S is the node O). We denote the height of S as h, and let the length of OD and OE be l_{OD} and l_{OE}, respectively. Then, it is easy to obtain the distances between S and D/E as

$$d_{SD} = \sqrt{h^2 + l_{OD}^2} \tag{1}$$

$$d_{SE} = \sqrt{h^2 + l_{OE}^2}, \tag{2}$$

respectively.

Also, the PDF of h can be presented as

$$f_h(x) = \frac{1}{H_{\max} - H_{\min}}, H_{\min} \le h \le H_{\max}, \tag{3}$$

where $H_{\max}$ and $H_{\min}$ are the maximum and minimum heights that S can reach, respectively.

In order to characterize the statistical characteristics of l_{OD} and l_{OE}, we use Fig. 3 to address the geometric relationships in the 3D space. As S is uniformly distributed in the 3D space, it is easy to obtain that O is uniformly distributed in the interval $[0, R_S]$ on the Y-axis. Then, we can easily achieve that the vertical distance from the project of S, O, to the highway AB is uniformly distributed variable, the PDF of p, which can be given as

$$f_p(x) = \begin{cases} \frac{1}{R_S}, & \text{if } 0 < x \le R_S \\ 0, & \text{else} \end{cases}. \tag{4}$$

In Fig. 2, we let the middle point of AB, C, as the origin, and AB as the horizontal axis, to facilitate the following analysis. Then, the coordinates of A and B can be written as $\left(\sqrt{R_S^2 - p^2}, 0\right)$ and $\left(-\sqrt{R_S^2 - p^2}, 0\right)$, respectively.

Therefore, when D and E are uniformly distributed on the line AB, conditioned on p, the conditional PDF of the length of CD and CE, t and w, can be presented as

$$f_{j|p}(x) = \begin{cases} \frac{1}{\sqrt{R_S^2 - p^2}}, & \text{if } 0 < x \le \sqrt{R_S^2 - p^2} \\ 0, & \text{else} \end{cases}, \tag{5}$$

where $j \in \{t, w\}$.

III. Secrecy Outage Analysis over Downlink

The received signal at D and E can be written as[2]

$$y_i = \sqrt{P_S / d_{Si}^{\alpha}} h_{Si} x_S + z_i, \tag{6}$$

where $i \in \{D, E\}$, P_S is the transmit power at S, d_{Si} is the distance between S and node i, h_{Si} is the channel gain over the link between S and node i, α is the path-loss factor. x_S is the information bit transmitted by S, z_i denotes the additive Gaussian white noise at node i with average power N_0.

The SNR at node i ($i \in \{D, E\}$) can be written as

$$\gamma_i = \frac{P_S |h_{Si}|^2}{N_0 d_{Si}^{\alpha}} = \frac{\lambda_{Si}}{d_{Si}^{\alpha}}, \tag{7}$$

[2] As the main purpose of this work is to uncover the impacts of the randomness of the positions of the UAV and vehicles, and small-scale fading on the secrecy outage performance of the considered system, the influence of Doppler shift is ignored for simplification purposes, which will be investigated in the future work.

where $\lambda_{Si} = \rho_S |h_{Si}|^2$ and $\rho_S = \frac{P_S}{N_0}$.

In this work, it is assumed that the channel between S and node i ($i \in \{D, E\}$) follows independent and identical Rician distribution. Then, the PDF and CDF of λ_{Si} can be expressed as [29]

$$f_{\lambda_{Si}}(x) = \exp(-\mu_i x) \sum_{n=0}^{\infty} A_i x^n, \tag{8}$$

$$F_{\lambda_{Si}}(x) = 1 - \exp(-\mu_i x) \sum_{l=0}^{\infty} \sum_{n=0}^{l} B_i x^n, \tag{9}$$

respectively, where $A_i = a_i \mu_i \exp(-K_i)$, $a_i = \frac{1}{(n!)^2} (K_i \mu_i)^n$, $\mu_i = \frac{1+K_i}{\Omega_{Si} \rho_S}$, $B_i = \frac{(K_i)^l (\mu_i)^n}{\exp(K_i) l! n!}$, Ω_{Si} is the fading power, and K_i is Rician factor corresponds to the ratio of the power of the LOS (specular) component to the average power of the scattered component. Although there is an infinite summation in (8) and (9), the expression of the CDF in (9) converges quickly to the finite series of summation, which has been testified in [29].

Therefore, the instantaneous secrecy capacity of the downlink transmission is

$$C_{\text{dn}}(\gamma_D, \gamma_E) = \max\{\log_2(1+\gamma_D) - \log_2(1+\gamma_E), 0\}. \tag{10}$$

In this work, passive eavesdropping is assumed to reflect the most common eavesdropping scenario for the eavesdropper to achieve the best eavesdropping and to keep itself from being uncovered. In other words, S has no CSI of the eavesdropping channel and SOP is investigated. Based on [15], SOP is defined as the probability that the secrecy capacity is smaller than a threshold R_{th}, which can be written as

$$\begin{aligned} P_{\text{out,dn}} &= \Pr\{C_{\text{dn}}(\gamma_D, \gamma_E) \le R_{\text{th}}\} \\ &= \Pr\{\gamma_D \le \Theta \gamma_E + \Theta - 1\} \\ &\ge \Pr\{\gamma_D \le \Theta \gamma_E\} = P^{\text{L}}_{\text{out,dn}}, \end{aligned} \tag{11}$$

where $\Theta = 2^{R_{\text{th}}}$.

A. Exact Secrecy Outage Analysis

Using (1), (2) and (7), one can rewrite the lower bound of SOP as

$$\begin{aligned} P^{\text{L}}_{\text{out,dn}} &= \Pr\{\gamma_D \le \Theta \gamma_E\} \\ &= \Pr\left\{\frac{\lambda_{SD}}{d_{SD}^{\alpha}} \le \Theta \frac{\lambda_{SE}}{d_{SE}^{\alpha}}\right\} \\ &= \Pr\left\{\frac{\lambda_{SD}}{\lambda_{SE}} \le \Theta \frac{(h^2+p^2+t^2)^{\frac{\alpha}{2}}}{(h^2+p^2+w^2)^{\frac{\alpha}{2}}}\right\} \\ &= \Pr\left\{X \le \Theta^{\frac{2}{\alpha}} Y\right\} \\ &= \int_0^{\infty} F_X\left(\Theta^{\frac{2}{\alpha}} y\right) f_Y(y)\, dy, \end{aligned} \tag{12}$$

where $X = \left(\frac{\lambda_{SD}}{\lambda_{SE}}\right)^{\frac{2}{\alpha}} = \left(\frac{|h_{SD}|^2}{|\lambda_{SE}|^2}\right)^{\frac{2}{\alpha}}$ and $Y = \frac{h^2+p^2+t^2}{h^2+p^2+w^2}$.

Remark 1: On can easily find that the lower bound of SOP given in (11) has nothing to do with the transmit SNR at S. In other words, increasing the transmit SNR at S is not a feasible way to improve the secrecy outage performance of the considered system.

Utilizing [35, Eq. (3.326.2)], we can derive the CDF of X as (13), shown on the top of next page.

Observing from Figs. 2 and 3, one can obtain $\phi_1 = \frac{H_{\min}^2}{H_{\min}^2 + R_S^2} \le Y \le \phi_1^{-1}$. To characterize the statistical characteristics of Y, a useful theorem is given as follows.

Theorem 1. *The PDF of* $Y = \frac{h^2+p^2+t^2}{h^2+p^2+w^2}$ *can be derived as*

$$f_Y(y) = \frac{1}{\Xi y^{1.5}} \times \begin{cases} \int_{H_{\min}}^{\sqrt{\frac{y}{1-y}} R_S} \int_0^{\sqrt{c_1 y - h^2}} g_1(p,h,y)\, dp dh, & \phi_1 \le y < \phi_2; \\ \int_{H_{\min}}^{H_{\max}} \int_0^{\sqrt{c_1 y - h^2}} g_1(p,h,y)\, dp dh, & \phi_2 \le y < 1; \\ \int_{H_{\min}}^{H_{\max}} \int_0^{\sqrt{\frac{c_1}{y} - h^2}} g_2(p,h,y)\, dp dh, & 1 < y \leqslant \frac{1}{\phi_2}; \\ \int_{H_{\min}}^{\sqrt{\frac{R_S^2}{y-1}}} \int_0^{\sqrt{\frac{c_1}{y} - h^2}} g_2(p,h,y)\, dp dh, & \frac{1}{\phi_2} < y \leqslant \frac{1}{\phi_1} \end{cases}, \tag{14}$$

where $g_1(p,h,y) = \frac{a_1(y+1)}{b_1} \log \frac{\sqrt{b_1 y} + \sqrt{c_1 y - a_1}}{\sqrt{a_1(1-y)}} + \sqrt{\frac{c_1 y^2 - a_1 y}{b_1}}$, $g_2(p,h,y) = \frac{a_1(y+1)}{b_1} \log \frac{\sqrt{b_1} + \sqrt{c_1 - a_1 y}}{\sqrt{a_1(y-1)}} + \sqrt{\frac{c_1 - a_1 y}{b_1}}$, $\Xi = 4R_S(H_{\max} - H_{\min})$, $a_1 = h^2 + p^2, b_1 = R_S^2 - p^2, c_1 = R_S^2 + h^2$, *and* $\phi_2 = \frac{H_{\max}^2}{H_{\max}^2 + R_S^2}$.

Proof: Please refer to the Appendix. ■

Substituting (13) and (14) into (12), we obtain

$$P^{\text{L}}_{\text{out,dn}} = 1 - \sum_{l=0}^{\infty} \sum_{n=0}^{l} \sum_{s=0}^{\infty} B_D A_E \Gamma(n+s+1) \Theta \psi, \tag{15}$$

where $\psi = \int_0^{\infty} \frac{y^{\iota_1}}{\tau^{n+s+1}} f_Y(y)\, dy$ with $\tau = \mu_E + \mu_D \Theta y^{\frac{\alpha}{2}}$ and $\iota_1 = \frac{\alpha n}{2}$. ψ can be written as (16), shown on the top of next page.

Using Chebyshev-Gauss quadrature method [36, Eq. (25.4.30)], we can have the approximated analytical expression of (16) as

$$\begin{aligned} \psi \approx\ & \frac{\hbar_1}{8\Xi} \sum_{k=1}^{N_3} \frac{\lambda_1 \eta_k \varepsilon_{k,1}{}^{\iota_1 - 1.5}}{T_{k,1}{}^{n+s+1}} \sum_{j=1}^{N_2} \upsilon_j \ell_1 \sum_{i=1}^{N_1} \xi_i G_1(\zeta_{i,1}, \vartheta_{j,1}, \varepsilon_{k,1}) \\ &+ \frac{\hbar_2}{8\Xi} \sum_{k=1}^{N_3} \frac{\lambda_2 \eta_k \varepsilon_{k,2}{}^{\iota_1 - 1.5}}{T_{k,2}{}^{n+s+1}} \sum_{j=1}^{N_2} \upsilon_j \ell_2 \sum_{i=1}^{N_1} \xi_i G_1(\zeta_{i,2}, \vartheta_{j,2}, \varepsilon_{k,2}) \\ &+ \frac{\hbar_3}{8\Xi} \sum_{k=1}^{N_3} \frac{\lambda_3 \eta_k \varepsilon_{k,3}{}^{\iota_1 - 1.5}}{T_{k,3}{}^{n+s+1}} \sum_{j=1}^{N_2} \upsilon_j \ell_3 \sum_{i=1}^{N_1} \xi_i G_2(\zeta_{i,3}, \vartheta_{j,3}, \varepsilon_{k,3}) \\ &+ \frac{\hbar_4}{8\Xi} \sum_{k=1}^{N_3} \frac{\lambda_4 \eta_k \varepsilon_{k,4}{}^{\iota_1 - 1.5}}{T_{k,4}{}^{n+s+1}} \sum_{j=1}^{N_2} \upsilon_j \ell_4 \sum_{i=1}^{N_1} \xi_i G_2(\zeta_{i,4}, \vartheta_{j,4}, \varepsilon_{k,4}), \end{aligned} \tag{17}$$

where N_1, N_2, and N_3 are the parameters for the summation item, which reflects accuracy vs. complexity,

$$\begin{aligned}\Pr\{X\le x\} &= \Pr\left\{\left(\frac{\lambda_{SD}}{\lambda_{SE}}\right)^{\frac{2}{\alpha}}\le x\right\} = \Pr\left\{\lambda_{SD}\le x^{\frac{\alpha}{2}}\lambda_{SE}\right\} = \int_0^{\infty} F_{\lambda_{SD}}\left(x^{\frac{\alpha}{2}}y\right) f_{\lambda_{SE}}(y)\,dy \\ &= \int_0^{\infty}\left(1-\exp\left(-\mu_D x^{\frac{\alpha}{2}}y\right)\sum_{l=0}^{\infty}\sum_{n=0}^{l} B_D\left(x^{\frac{\alpha}{2}}y\right)^n\right)\exp\left(-\mu_E y\right)\sum_{s=0}^{\infty} A_E y^s dy \\ &= 1-\sum_{l=0}^{\infty}\sum_{n=0}^{l} B_D\left(x^{\frac{\alpha}{2}}\right)^n\sum_{s=0}^{\infty} A_E\int_0^{\infty} y^{n+s}\exp\left(-\left(\mu_E+\mu_D x^{\frac{\alpha}{2}}\right)y\right)dy \\ &= 1-\sum_{l=0}^{\infty}\sum_{n=0}^{l}\sum_{s=0}^{\infty} B_D A_E\left(x^{\frac{\alpha}{2}}\right)^n\frac{\Gamma(n+s+1)}{\left(\mu_E+\mu_D x^{\frac{\alpha}{2}}\right)^{n+s+1}}\end{aligned} \tag{13}$$

$$\begin{aligned}\psi = &\frac{1}{\Xi}\int_{\phi_1}^{\phi_2}\frac{y^{\iota_1-1.5}}{\tau^{n+s+1}}\int_{H_{\min}}^{\sqrt{\frac{R_S^2 y}{1-y}}}\int_0^{\sqrt{c_1 y-h^2}} g_1(p,h,y)\,dpdhdy + \frac{1}{\Xi}\int_{\phi_2}^{1}\frac{y^{\iota_1-1.5}}{\tau^{n+s+1}}\int_{H_{\min}}^{H_{\max}}\int_0^{\sqrt{c_1 y-h^2}} g_1(p,h,y)\,dpdhdy \\ &+\frac{1}{\Xi}\int_{1}^{\frac{1}{\phi_2}}\frac{y^{\iota_1-1.5}}{\tau^{n+s+1}}\int_{H_{\min}}^{H_{\max}}\int_0^{\sqrt{\frac{c_1}{y}-h^2}} g_2(p,h,y)\,dpdhdy + \frac{1}{\Xi}\int_{\frac{1}{\phi_2}}^{\frac{1}{\phi_1}}\frac{y^{\iota_1-1.5}}{\tau^{n+s+1}}\int_{H_{\min}}^{\sqrt{\frac{R_S^2}{y-1}}}\int_0^{\sqrt{\frac{c_1}{y}-h^2}} g_2(p,h,y)\,dpdhdy\end{aligned} \tag{16}$$

$\hbar_1 = \phi_2-\phi_1$, $\hbar_2 = 1-\phi_2$, $\hbar_3 = \frac{1}{\phi_2}-1$, $\hbar_4 = \frac{1}{\phi_1}-\frac{1}{\phi_2}$, $\lambda_1 = \sqrt{\frac{R_S^2\varepsilon_{k,1}}{1-\varepsilon_{k,1}}} - H_{\min}$, $\lambda_2 = \lambda_3 = H_{\max}-H_{\min}$, $\lambda_4 = \sqrt{\frac{R_S^2}{\varepsilon_{k,4}-1}} - H_{\min}$, η_k, υ_j, ξ_i are the Gaussian weights, which are constants and given in [31, Table (25.4)], $\varepsilon_{k,s} = \frac{\hbar_s}{2}z_s+\varrho_s$, $s=1,2,3,4$, $\varrho_1 = \frac{\phi_1+\phi_2}{2}$, $\varrho_2 = \frac{1+\phi_2}{2}$, $\varrho_3 = \frac{1}{2}(1+\frac{1}{\phi_2})$, $\varrho_4 = \frac{1}{2}(\frac{1}{\phi_1}+\frac{1}{\phi_2})$, $T_{k,s} = \mu_E+\mu_D\Theta\varepsilon_{k,s}^{\frac{\alpha}{2}}$, $C_{1,s} = R_S^2+{\vartheta_{j,s}}^2$, $\vartheta_{j,s} = \frac{\lambda_s}{2}y_s+\chi_s$, $\chi_1 = \frac{1}{2}(H_{\min}+\sqrt{\frac{R_S^2\varepsilon_{k,1}}{1-\varepsilon_{k,1}}})$, $\chi_2 = \chi_3 = \frac{1}{2}(H_{\min}+H_{\max})$, $\chi_4 = \frac{1}{2}(H_{\min}+\sqrt{\frac{R_S^2}{\varepsilon_{k,4}-1}})$, $\ell_t = \sqrt{C_{1,t}\varepsilon_{k,t}-{\vartheta_{j,t}}^2}$, $t = 1,2$; $\ell_t = \sqrt{\frac{C_{1,t}}{\varepsilon_{k,t}}-{\vartheta_{j,t}}^2}$, $t = 3,4$, $\zeta_{i,s} = \frac{\ell_s}{2}x_s+\frac{\ell_s}{2}$, $G_1(\zeta_{i,s},\vartheta_{j,s},\varepsilon_{k,s}) = \sqrt{\frac{C_{1,s}{\varepsilon_{k,s}}^2-A_{1,s}\varepsilon_{k,s}}{B_{1,s}}} + \frac{A_{1,s}(\varepsilon_{k,s}+1)}{B_{1,s}}\log\frac{\sqrt{B_{1,s}\varepsilon_{k,s}}+\sqrt{C_{1,s}\varepsilon_{k,s}-A_{1,s}}}{\sqrt{A_{1,s}(1-\varepsilon_{k,s})}}$, $G_2(\zeta_{i,s},\vartheta_{j,s},\varepsilon_{k,s}) = \frac{A_{1,s}(\varepsilon_{k,s}+1)}{B_{1,s}}\log\frac{\sqrt{B_{1,s}}+\sqrt{C_{1,s}-A_{1,s}\varepsilon_{k,s}}}{\sqrt{A_{1,s}(\varepsilon_{k,s}-1)}} + \sqrt{\frac{C_{1,s}-A_{1,s}\varepsilon_{k,s}}{B_{1,s}}}$ with $A_{1,s} = {\vartheta_{j,s}}^2+{\zeta_{i,s}}^2$, $B_{1,s} = R_S^2-{\zeta_{i,s}}^2$, x_s, y_s, z_s are the sth zeros of Legendre polynomials, which are given in [36, Table (25.4)].

B. Asymptotic Secrecy Outage Analysis

To obtain a simplified expression for SOP, in this section we analyze the asymptotic SOP of the UAV-2-V communication systems in the high-Ω_{SD} regime. When $\Omega_D\to\infty$, applying [29, Eq. (26)], we obtain the asymptotic CDF of λ_{SD} as

$$F_{\lambda_{SD}}^{\infty}(x) = \mu_D\exp(-K_D)\,x\exp(-\mu_D x). \tag{18}$$

Utilizing [35, Eq. (3.326.2)], the asymptotic CDF of X is expressed as

$$F_X^{\infty}(x) = \mu_D\exp(-K_D)\,x^{\frac{\alpha}{2}}\sum_{s=0}^{\infty}\frac{A_E\Gamma(s+2)}{\left(\mu_E+\mu_D x^{\frac{\alpha}{2}}\right)^{s+2}}. \tag{19}$$

Thus, the asymptotic SOP is obtained as

$$\begin{aligned}P_{\text{out,dn}}^{\text{L},\infty} &= \int_0^{\infty} F_X^{\infty}\left(\Theta^{\frac{2}{\alpha}}y\right) f_Y(y)\,dy \\ &= \mu_D\exp(-K_D)\,\Theta\sum_{s=0}^{\infty}\frac{A_E\Gamma(s+2)}{(\mu_E)^{s+2}}\psi^{\infty},\end{aligned} \tag{20}$$

where ψ^{∞} is shown as (21) on the top of next page.

Similar to (17), we can finally derive ψ^{∞} as (22) shown on the top of next page.

IV. Secrecy Outage Analysis over Uplink

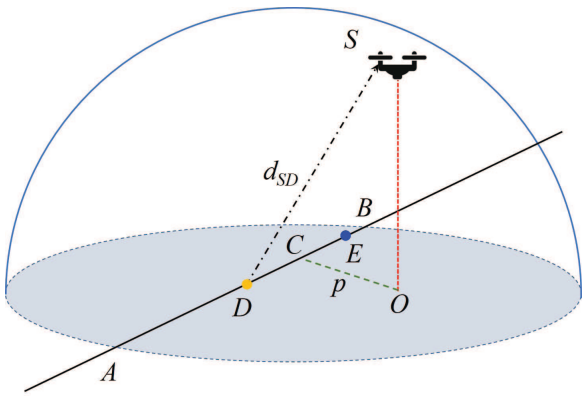

Fig. 4: 3D model for V-2-UAV link

$$\psi^{\infty} = \frac{1}{\Xi}\int_{\phi_1}^{\phi_2} y^{\frac{\alpha-3}{2}} \int_{H_{\min}}^{\sqrt{\frac{R_S^2 y}{1-y}}} \int_{0}^{\sqrt{c_1 y - h^2}} g_1(p,h,y)\, dpdhdy + \frac{1}{\Xi}\int_{\phi_2}^{1} y^{\frac{\alpha-3}{2}} \int_{H_{\min}}^{H_{\max}} \int_{0}^{\sqrt{c_1 y - h^2}} g_1(p,h,y)\, dpdhdy$$
$$+ \frac{1}{\Xi}\int_{1}^{\frac{1}{\phi_2}} y^{\frac{\alpha-3}{2}} \int_{H_{\min}}^{H_{\max}} \int_{0}^{\sqrt{\frac{c_1}{y} - h^2}} g_2(p,h,y)\, dpdhdy + \frac{1}{\Xi}\int_{\frac{1}{\phi_2}}^{\frac{1}{\phi_1}} y^{\frac{\alpha-3}{2}} \int_{H_{\min}}^{\sqrt{\frac{R_S^2}{y-1}}} \int_{0}^{\sqrt{\frac{c_1}{y} - h^2}} g_2(p,h,y)\, dpdhdy. \tag{21}$$

$$\psi^{\infty} \approx \frac{\hbar_1}{8\Xi}\sum_{k=1}^{N_3} \lambda_1 \eta_k \varepsilon_{k,1}{}^{0.5\alpha-1.5} \sum_{j=1}^{N_2} \upsilon_j \ell_1 \sum_{i=1}^{N_1} \xi_i G_1(\zeta_{i,1}, \vartheta_{j,1}, \varepsilon_{k,1}) + \frac{\hbar_2}{8\Xi}\sum_{k=1}^{N_3} \lambda_2 \eta_k \varepsilon_{k,2}{}^{0.5\alpha-1.5} \sum_{j=1}^{N_2} \upsilon_j \ell_2 \sum_{i=1}^{N_1} \xi_i G_1(\zeta_{i,2}, \vartheta_{j,2}, \varepsilon_{k,2})$$
$$+ \frac{\hbar_3}{8\Xi}\sum_{k=1}^{N_3} \lambda_3 \eta_k \varepsilon_{k,3}{}^{0.5\alpha-1.5} \sum_{j=1}^{N_2} \upsilon_j \ell_3 \sum_{i=1}^{N_1} \xi_i G_2(\zeta_{i,3}, \vartheta_{j,3}, \varepsilon_{k,3}) + \frac{\hbar_4}{8\Xi}\sum_{k=1}^{N_3} \lambda_4 \eta_k \varepsilon_{k,4}{}^{0.5\alpha-1.5} \sum_{j=1}^{N_2} \upsilon_j \ell_4 \sum_{i=1}^{N_1} \xi_i G_2(\zeta_{i,4}, \vartheta_{j,4}, \varepsilon_{k,4}) \tag{22}$$

In Fig. 4, we present the 3D model for the transmission over V-2-UAV link to aid the following analysis in this section. The coverage space of D is a hemisphere with the centre D and radius $R_D = AD = DB$.

In order to address the randomness of the positions of both D and E, we take D as the origin and it is assumed that E is uniformly distributed on the line segment AB with length L_{AB}. Then, the PDF of d_{DE} can be presented as

$$f_{d_{DE}}(x) = \begin{cases} \frac{1}{R_D}, & \text{if } 0 < x \le R_D \\ 0, & \text{else} \end{cases}. \tag{23}$$

During the uplink transmission stage, S is uniformly distributed in the coverage space of D. Therefore, the PDF of the distance between D and S can be written as

$$f_{d_{DS}}(x) = \begin{cases} \frac{3x^2}{R_D^3}, & \text{if } 0 < x \le R_D \\ 0, & \text{else} \end{cases}. \tag{24}$$

The received signal at S/E can be written as

$$y_j = \sqrt{P_D / d_{Dj}^{\alpha}} h_{Dj} x_D + z_j, \tag{25}$$

where $j \in \{S, E\}$, P_D is the transmit power at D, d_{Dj} is the distance between D and node j, h_{Dj} is the channel gain over the link between D and node j, x_D is the information bits transmitted by D, z_j is the additional Gaussian white noise at node j with average power N_0. For simplification purposes, in this work we assume that h_{DS} has the same statistical characteristics with h_{SD} due to reciprocity of the wireless channels.

Accordingly, the received SNR at node j ($j \in \{S, E\}$) can be written as

$$\gamma_j = \frac{P_D |h_{Dj}|^2}{N_0 d_{Dj}^{\alpha}} = \frac{\lambda_{Dj}}{d_{Dj}^{\alpha}}, \tag{26}$$

where $\lambda_{Dj} = \rho_D |h_{Dj}|^2$ and $\rho_D = \frac{P_D}{N_0}$. Moreover, we also have $\lambda_{DS} = \lambda_{SD}$ by considering the reciprocity of the wireless channels.

Similarly, the SOP over the uplink is given as

$$P_{\text{out,up}}^{\text{L}} = \Pr\{\gamma_S \le \Theta \gamma_E\} = \Pr\left\{ \frac{\lambda_{DS}}{d_{DS}^{\alpha}} \le \Theta \frac{\lambda_{DE}}{d_{DE}^{\alpha}} \right\}. \tag{27}$$

Clearly, in this case, the link between D and E is a vehicle-to-vehicle (V2V) link. As discussed in [37], Rician fading is used to statistically describe the V2V communication in urban, suburban, and highway environments, when the distance between communicating vehicles is small and a strong LOS component is present. However, when the vehicle separation increases, the fading gradually transits from Rician to Rayleigh. Moreover, when the distance exceeds 70-100 m, the fading becomes worse than Rayleigh, modeled as Weibull fading. Hence, for V2V communications, it is reasonable and practical that different fading models may be applicable according to the surrounding environment and the vehicle density.

To fully cover all potential cases, in this work we will carry out our analysis work for two cases: 1) $D - E$ link suffers Rician fading; 2) $D - E$ link suffers Weibull fading.

A. $D - E$ Link Suffering Rician Fading

In this case, the SNR at S and E can be expressed as $\gamma_S = \frac{\rho_D |h_{DS}|^2}{d_{DS}^{\alpha}} = \frac{\lambda_{DS}}{d_{DS}^{\alpha}}$ and $\gamma_E = \frac{\rho_D |h_{DE}|^2}{d_{DE}^{\alpha}} = \frac{\lambda_{DE}}{d_{DE}^{\alpha}}$, respectively, where $\lambda_{DS} = \rho_D |h_{DS}|^2$ and $\lambda_{DE} = \rho_D |h_{DE}|^2$.

Using [38, Eq. (5)], we have the PDF of d_{DS}^{α} as

$$f_{d_{DS}^{\alpha}}(t) = \frac{\varpi}{R_D^3} t^{\varpi - 1}, \ 0 < t \le R_D^{\alpha}, \tag{28}$$

where $\varpi = \frac{3}{\alpha}$.

Utilizing [35, Eq. (3.351.1)], the CDF of γ_S is obtained as

$$\begin{aligned}F_{\gamma_S}(x) &= \Pr\{\gamma_S \le x\} = \Pr\{\lambda_{DS} \le d_{DS}^{\alpha} x\} \\ &= \int_0^{\infty} F_{\lambda_{DS}}(tx) f_{d_{DS}^{\alpha}}(t)\, dt \\ &= 1 - \sum_{l=0}^{\infty}\sum_{n=0}^{l} B_{DS} x^n \int_0^{\infty} t^n \exp(-\mu_{DS} t x) f_{d_{DS}^{\alpha}}(t)\, dt \\ &= 1 - \frac{3}{\alpha R_D^3}\sum_{l=0}^{\infty}\sum_{n=0}^{l} B_{DS} x^n \\ &\quad \times \int_0^{R_D^{\alpha}} t^{n+\varpi-1}\exp(-\mu_{DS} t x)\, dt \\ &= 1 - \sum_{l=0}^{\infty}\sum_{n=0}^{l} \beta_S x^{-\varpi} \Upsilon(n+\varpi, \phi_S x), \end{aligned} \tag{29}$$

where $\beta_S = \frac{\varpi B_{DS}}{(\mu_{DS})^{n+\varpi} R_D^3}$, $\phi_S = \mu_{DS} R_D^{\alpha}$, $\mu_{DS} = \frac{1+K_{DS}}{\Omega_{DS}\rho_D}$, $B_{DS} = \frac{(K_{DS})^l (\mu_{DS})^n}{\exp(K_{DS}) l! n!}$, Ω_{DS} is the fading power, and K_{DS} is the Rician factor for λ_{DS}.

Similarly, unitizing [35, Eq. (3.351.1)], we have the PDF of γ_E as

$$\begin{aligned}f_{\gamma_E}(x) &= \int_0^{\infty} f_{\lambda_{DE}}(xy) f_{d_{DE}^{\alpha}}(y)\, y dy \\ &= \sum_{s=0}^{\infty} A_{DE} x^s \frac{\gamma}{R_D} \int_0^{R_D^{\alpha}} y^{s+\gamma}\exp(-\mu_{DE} x y)\, dy \\ &= \sum_{s=0}^{\infty} \beta_E x^{-\gamma-1} \Upsilon(s+\gamma+1, \phi_E x), \end{aligned} \tag{30}$$

where $\gamma = \frac{1}{\alpha}$, $\beta_E = \frac{\tau A_{DE} (\mu_{DE})^{-s-\gamma-1}}{R_D}$, $\mu_{DE} = \frac{1+K_{DE}}{\Omega_{DE}\rho_D}$, $A_{DE} = a_{DE}\mu_{DE}\exp(-K_{DE})$, $a_{DE} = \frac{1}{(s!)^2}(K_{DE}\mu_{DE})^s$, $\phi_E = \mu_{DE} R_D^{\alpha}$, Ω_{DE} is the fading power, and K_{DE} is the Rician factor for λ_{DE}.

Employing [39, Eq. (8.4.16.1)] and [40, Eq. (12)], the SOP in this case is obtained as

$$\begin{aligned}P_{\text{out,up}}^{\text{L}} &= \Pr\{\gamma_S \le \Theta\gamma_E\} = \int_0^{\infty} F_{\gamma_S}(\Theta x) f_{\gamma_E}(x)\, dt \\ &= 1 - \sum_{l=0}^{\infty}\sum_{n=0}^{l} \beta_S \Theta^{-\varpi} \sum_{s=0}^{\infty} \beta_E \int_0^{\infty} x^{-\varpi-\gamma-1} \\ &\quad \times \Upsilon(s+\gamma+1, \phi_E x)\Upsilon(n+\varpi, \Theta\phi_S x)\, dx \\ &= 1 - \sum_{l=0}^{\infty}\sum_{n=0}^{l} \beta_S \Theta^{-\varpi} \sum_{s=0}^{\infty} \beta_E {\phi_E}^{\varpi+\gamma} \\ &\quad \times G_{3,3}^{2,2}\left[\frac{\Theta\phi_S}{\phi_E}\middle| \begin{matrix} 1, \varpi - s, 1+\varpi+\gamma \\ n+\varpi, \varpi+\gamma, 0 \end{matrix}\right], \end{aligned} \tag{31}$$

where $G_{p,q}^{m,n}\left[x\middle|\begin{matrix} a_1,\cdots,a_p \\ b_1,\cdots,b_q \end{matrix}\right]$ is the Meijer's G-function, as defined by [35, Eq. (9.301)].

Using [35, Eq. (1.4.13)] and $\lim_{z\to 0^+} {}_pF_q(a,b,z) = 1$ [41], for Meijer-G function, it is known that

$$\begin{aligned}&\lim_{x\to 0} G_{p,q}^{m,n}\left[x\middle|\begin{matrix} a_1,\cdots,a_p \\ b_1,\cdots,b_q \end{matrix}\right] \\ &= \sum_{k=1}^{m} \frac{\prod_{j=1, j\ne k}^{m}\Gamma(b_j - b_k)\prod_{j=1}^{n}\Gamma(1+b_k-a_j)}{\prod_{j=n+1}^{p}\Gamma(a_j-b_k)\prod_{j=m+1}^{q}\Gamma(1+b_k-b_j)} x^{b_k} + o\left(x^{b_k}\right), \end{aligned} \tag{32}$$

if $p \le q$ and for $1 \le j,k \le m, j \ne k$, $b_j - b_k \notin \mathbb{Z}$ hold. Then, when $x \to 0$, we can have

$$\begin{aligned}&G_{3,3}^{2,2}\left[x\middle|\begin{matrix} 1, \varpi - s, 1+\varpi+\gamma \\ n+\varpi, \varpi+\gamma, 0 \end{matrix}\right] \\ &= \begin{cases} \frac{s!}{\gamma\varpi} x^{\varpi} + \frac{\Gamma(-\gamma)\Gamma(1+s+\gamma)}{\varpi+\gamma} x^{\varpi+\gamma} + o(x^{\varpi+\gamma}), & n = 0; \\ \frac{\Gamma(n-\gamma)\Gamma(1+s+\gamma)}{\varpi+\gamma} x^{\varpi+\gamma} + o(x^{\varpi+\gamma}), & n \ne 0 \end{cases}. \end{aligned} \tag{33}$$

Thus, when $\Omega_{DS} \to \infty$, the asymptotic SOP, in this case, is obtained as (34), shown on the top of next page.

Based on the definition of the secrecy diversity order (SDO) presented in [42], we can derive the SDO in this case as

$$G_d = \gamma = \frac{1}{\alpha}. \tag{35}$$

B. $D-E$ Link Suffering Weibull Fading

In this case, we have $\gamma_E = \frac{\rho_D |h_{DE}|^2}{d_{DE}^{\alpha}} = \frac{\lambda_{DE}}{d_{DE}^{\alpha}}$. The PDF of the power gain over $D-E$ link $|h_{DE}|^2$ is

$$f_{|h_{DE}|^2}(x) = \frac{b}{a^b} x^{b-1}\exp\left(-\frac{x^b}{a^b}\right), \tag{36}$$

where a is the scale parameter, b is the Weibull fading parameter[3]. When $b = 1$, the Weibull distribution becomes an exponential distribution; $b = 2$ implies the well-known Rayleigh distribution. Then, the PDF of λ_{DE} is obtained as

$$f_{\lambda_{DE}}(x) = \frac{b}{(\rho_D a)^b} x^{b-1}\exp\left(-\frac{x^b}{(\rho_D a)^b}\right). \tag{37}$$

Thus, we can further have the CDF of d_{DE}^{α} as

$$F_{d_{DE}^{\alpha}}(x) = \Pr\{d_{DE}^{\alpha} \le x\} = \begin{cases} \frac{x^{\gamma}}{R_D}, & \text{if } 0 < x \le R_D^{\alpha}; \\ 1, & \text{elseif } x > R_D^{\alpha}; \\ 0, & \text{else} \end{cases}. \tag{38}$$

Using (38), we obtain the PDF of d_{DE}^{α} as

$$f_{d_{DE}^{\alpha}}(x) = \frac{\gamma x^{\gamma-1}}{R_D}, 0 < x \le R_D^{\alpha}. \tag{39}$$

[3]In this work, we only consider the case that $b \in \mathbb{Z}^+$ for mathematical tractability.

$$
\begin{aligned}
P_{\text{out,up}}^{\text{L},\infty} &= 1-\sum_{l=0}^{\infty}\sum_{n=0}^{l}\beta_S\Theta^{-\varpi}\sum_{s=0}^{\infty}\beta_E\phi_E{}^{\varpi+\gamma}\times G_{3,3}^{2,2}\left[\frac{\Theta\phi_S}{\phi_E}\middle|\begin{matrix}1,\varpi-s,1+\varpi+\gamma\\ n+\varpi,\varpi+\gamma,0\end{matrix}\right]\\
&= 1-\underbrace{\sum_{l=0}^{\infty}\beta_S\Theta^{-\varpi}\sum_{s=0}^{\infty}\beta_E\phi_E{}^{\varpi+\gamma}\times G_{3,3}^{2,2}\left[\frac{\Theta\phi_S}{\phi_E}\middle|\begin{matrix}1,\varpi-s,1+\varpi+\gamma\\ \varpi,\varpi+\gamma,0\end{matrix}\right]}_{n=0}\\
&\quad-\underbrace{\sum_{l=1}^{\infty}\sum_{n=1}^{l}\beta_S\Theta^{-\varpi}\sum_{s=0}^{\infty}\beta_E\phi_E{}^{\varpi+\gamma}\times G_{3,3}^{2,2}\left[\frac{\Theta\phi_S}{\phi_E}\middle|\begin{matrix}1,\varpi-s,1+\varpi+\gamma\\ n+\varpi,\varpi+\gamma,0\end{matrix}\right]}_{n\neq 0}\\
&\overset{(33)}{=} -\left(\frac{\Theta\phi_S}{\phi_E}\right)^{\gamma}\sum_{l=0}^{\infty}\sum_{n=0}^{l}\sum_{s=0}^{\infty}\frac{\gamma\varpi(K_{DS})^{l}(K_{DE})^{s}\Gamma(n-\gamma)\Gamma(1+s+\gamma)}{\exp(K_{DS}+K_{DE})\,l!n!(s!)^{2}(\varpi+\gamma)}+o\left((\phi_S)^{\gamma}\right)
\end{aligned}
\tag{34}
$$

So, the PDF of $\gamma_E=\frac{\rho_D|h_{DE}|^2}{d_{DE}^{\alpha}}$ can be derived as

$$
\begin{aligned}
f_{\gamma_E}(x) &= \int_0^{\infty} f_{\lambda_{DE}}(xy)\, f_{d_{DE}^{\alpha}}(y)\, y dy\\
&= \frac{b}{(\rho_D a)^b}\frac{\gamma}{R_D}x^{b-1}\int_0^{R_D^{\alpha}} y^{\gamma+b-1}\exp\left(-\frac{x^b}{(\rho_D a)^b}y^b\right)dy\\
&= \frac{(\rho_D a)^{\gamma}\gamma}{R_D}x^{-\gamma-1}\Upsilon\left(\frac{\tau}{b}+1,\frac{x^b}{(\rho_D a)^b}(R_D)^{\frac{\alpha}{b}}\right)\\
&= \tilde{A}_{DE}x^{-\gamma-1}\Upsilon\left(\frac{\gamma}{b}+1,\tilde{B}_{DE}x^b\right),
\end{aligned}
\tag{40}
$$

where $\tilde{A}_{DE}=\frac{(\rho_D a)^{\gamma}\gamma}{R_D}$ and $\tilde{B}_{DE}=\frac{R_D^{\frac{\alpha}{b}}}{(\rho_D a)^b}$.

Thus, adopting [40, Eq. (21)], the SOP in this case is finally written as (41), shown on the top of next page, where $\Delta(k,a)=\frac{a}{k},\frac{a+1}{k},...,\frac{a+k-1}{k}$ with β_S and ϕ_S defined in (29).

For Meijer-G function, as indicated by [43, Eq. (A.1)], when $x\to\infty$, we have

$$
\begin{aligned}
&\lim_{x\to\infty} G_{p,q}^{m,n}\left[x\middle|\begin{matrix}a_1,\cdots,a_p\\ b_1,\cdots,b_q\end{matrix}\right]\\
&= \sum_{k=1}^{n}\frac{\prod_{j=1,j\neq k}^{n}\Gamma(a_k-a_j)\prod_{j=1}^{m}\Gamma(1+b_j-a_k)}{\prod_{j=n+1}^{p}\Gamma(1+a_j-a_k)\prod_{j=m+1}^{q}\Gamma(a_k-b_j)}\\
&\quad\times x^{a_k-1}\left(1+O\left(\frac{1}{x}\right)\right),
\end{aligned}
\tag{42}
$$

where $p\geq q$ and $a_k-a_l\notin\mathbb{Z},(k,l=1,2,\cdots,n,k\neq l)$.

Similar to the derivation of (34), the asymptotic SOP and the SDO in this case are obtained as (43) shown on the top of next page, and

$$
G_d=\gamma=\frac{1}{\alpha},
\tag{44}
$$

respectively.

V. Numerical Results and Discussion

In this section, Monte Carlo simulations are carried out to validate our proposed analytical expressions for the SOP over both downlink and uplink. The main parameters are set as $H_{\max}=50$ m, $H_{\min}=10$ m, $R_S=100$ m, $\rho_S=40$ dB, $\Omega_{SE}=1$, $K_{DS}=K_{DE}=2$, $\alpha=3$, $R_{\text{th}}=1$ bits/s/Hz, $R_D=100$ m, $a=0.5$, and $b=1$. We run 10^5 trials for the Monte Carlo simulations and also consider 10^5 times of the realizations of the considered systems.

A. Secrecy Outage Analysis of Downlink

In this subsection, the SOP in the downlink of the considered system will be investigated in Figs. 5 - 8.

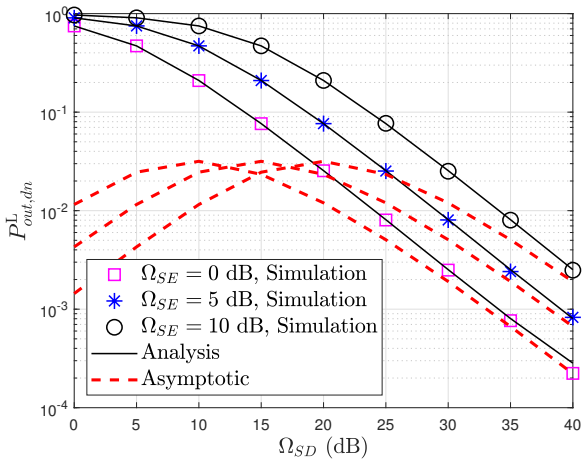

Fig. 5: SOP vs. Ω_{SD} for various Ω_{SE}.

In the first experiment, the impact of the received signal variance at the eavesdropper Ω_{SE} on the SOP was studied and shown in Fig. 5. We can see that SOP decreases as Ω_{SE} increases, which shows Ω_{SE} offers a negative effect on SOP. This is because a larger Ω_{SE} gives a better channel condition for the eavesdropping link between S and E. Moreover, the asymptotic SOP of the considered system gets close to the simulation and analysis ones as the average channel gain increases.

In Figs. 6 and 7, we present simulation and analytical results of SOP vs. main-to-eavesdropper ratio (MER), which is defined as Ω_{SD}/Ω_{SE}, to address the impact of the maximum and minimum heights that S can reach, respectively. $H_{\max}$ and $H_{\min}$ do not exhibit a significant influence on SOP,

$$P_{\text{out,up}}^{\text{L}} = \Pr\left\{\gamma_S \le \Theta\gamma_E\right\} = \int_0^\infty F_{\gamma_S}\left(\Theta x\right) f_{\gamma_E}\left(x\right) dt$$
$$= 1 - \tilde{A}_{DE} \sum_{l=0}^{\infty}\sum_{n=0}^{l} \beta_S \Theta^{-\varpi} \int_0^\infty x^{-\gamma-\varpi-1} \Upsilon\left(n+\varpi, \phi_S\Theta x\right) \Upsilon\left(\frac{\gamma}{b}+1, \tilde{B}_{DE}x^b\right) dx$$
$$= 1 - \tilde{A}_{DE} \sum_{l=0}^{\infty}\sum_{n=0}^{l} \beta_S \Theta^{-\varpi} \int_0^\infty x^{-\gamma-\varpi-1} G_{1,2}^{1,1}\left[\phi_S\Theta x \left|{}^{1}_{n+\varpi,0}\right.\right] G_{1,2}^{1,1}\left[\tilde{B}_{DE}x^b \left|{}^{1}_{\frac{\gamma}{b}+1,0}\right.\right] dx$$
$$= 1 - \frac{\tilde{A}_{DE}\Theta^{\gamma} b^{-\gamma-1.5}}{(2\pi)^{0.5(b-1)}} \sum_{l=0}^{\infty}\sum_{n=0}^{l} b^n \beta_S (\phi_S)^{\gamma+\varpi} G_{1+2b,2+b}^{1+b,1+b}\left[\frac{\tilde{B}_{DE}b^b}{(\phi_S\Theta)^b} \left|{}^{1,\Delta(b,1+\gamma-n),\Delta(b,1+\gamma+\varpi)}_{\Delta\left(1,\frac{\gamma}{b}+1\right),\Delta(b,\gamma+\varpi),0}\right.\right] \tag{41}$$

$$P_{\text{out,up}}^{\text{L},\infty} = -\frac{\varpi\tilde{A}_{DE}(\Theta\phi_S)^{\gamma} b^{-\gamma-0.5}}{(2\pi)^{0.5(b-1)}\exp\left(K_{DS}\right)} \sum_{l=0}^{\infty}\sum_{n=0}^{l} \frac{\Gamma\left(1-\Delta\left(b,1+\gamma-n\right)\right)\Gamma\left(\frac{\gamma}{b}+1\right)}{b^{-n}(K_{DS})^{-l} l!n!\left(\gamma+\varpi\right)} + o\left((\phi_S)^{\gamma}\right) \tag{43}$$

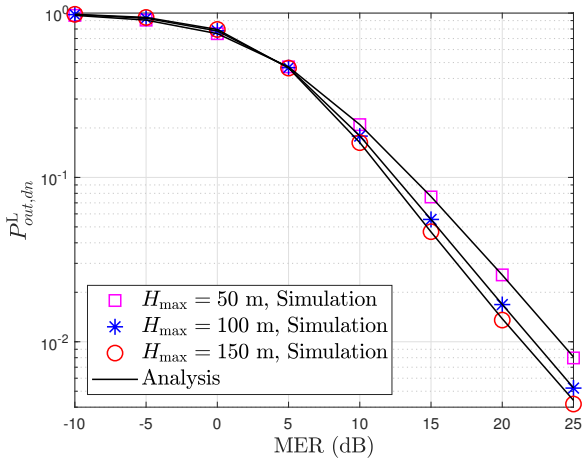

Fig. 6: SOP vs. MER for various $H_{\max}$.

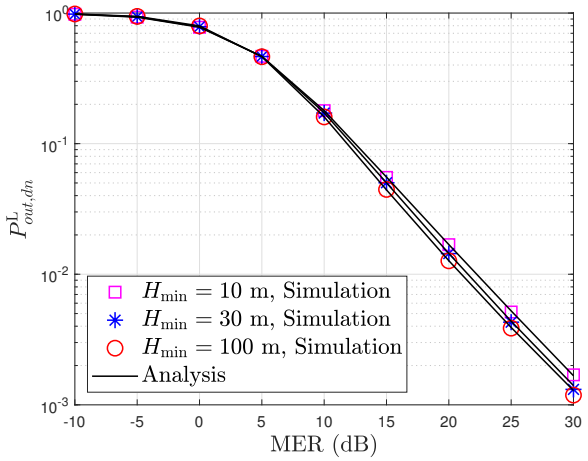

Fig. 7: SOP vs. MER for various $H_{\min}$.

while a large $H_{\max}/H_{\min}$ incurs the improved secrecy outage performance. We can then have that the altitude of S shows a positive effect on SOP but not an effective way.

Fig. 8 presents the secrecy outage performance of the

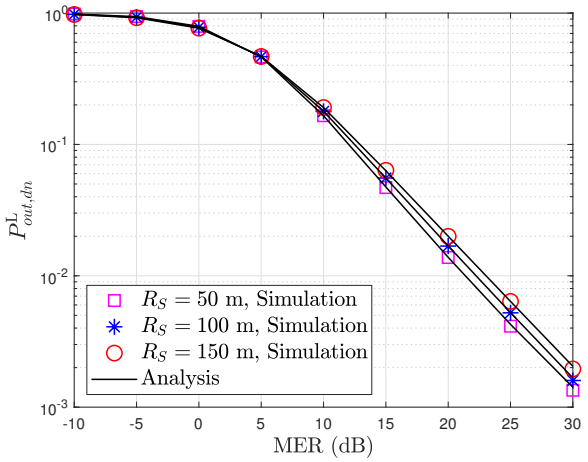

Fig. 8: SOP vs. MER for various R_S.

considered system, while varying the radius of the coverage area on the ground of S, $R_S = 150, 100$, and 50 m. One can find that R_S exhibits a negative effect on SOP, which comes from the fact that a large R_S leads to a large coverage area of S, and then the probability that the distance d_{SE} gets large increases, which results in the received signal power loss at E.

B. Secrecy Outage Analysis Over Uplink

In this subsection, we will study the SOP over the uplink of the considered system shown in Fig. 4 when D-E link suffers Rician and Weibull fading, respectively.

1) D-E link suffering Rician Fading: Fig. 9 depicts the SOP with various mean values of the power gain over D-E link, Ω_{DE}, while Ω_{DS} increasing. The SOP with a small Ω_{DE} outperforms that with a large Ω_{DE}, as a large Ω_{DE} represents a higher channel gain for the eavesdropping link. This observation is also similar to the one obtained for the downlink.

2) D-E link suffering Weibull Fading: Considering that the channel between D and E experences Weibull fading, Fig.

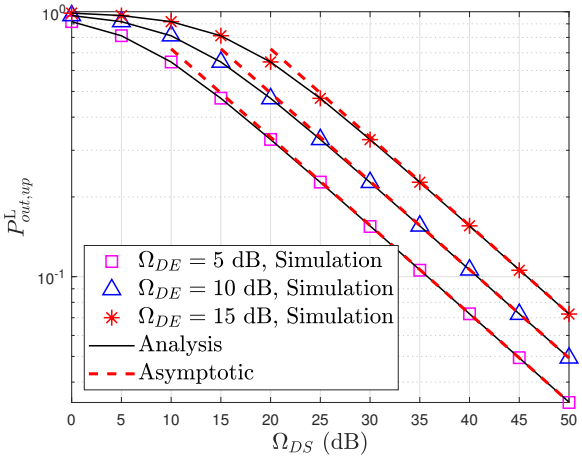

Fig. 9: SOP vs. Ω_{DS} for various Ω_{DE}.

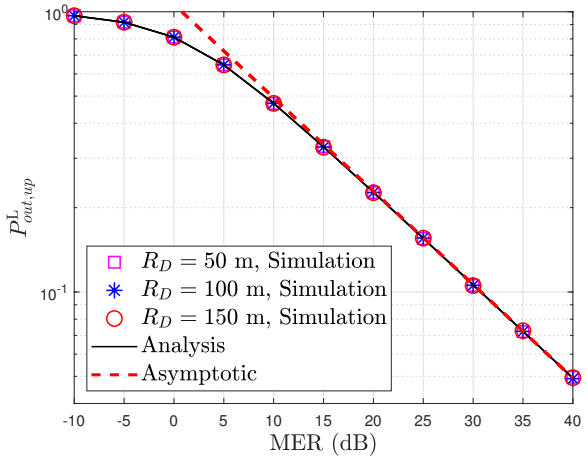

Fig. 11: SOP vs. MER for various R_D.

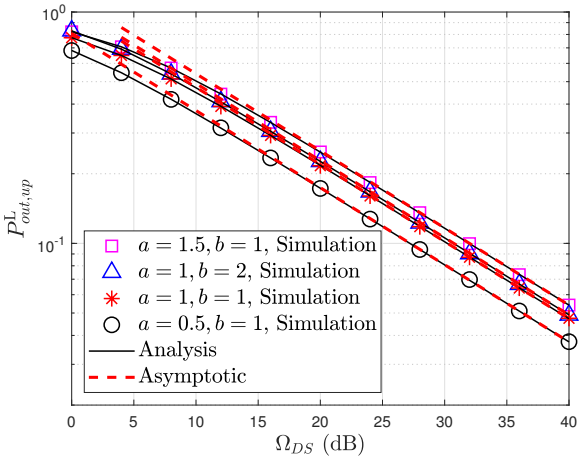

Fig. 10: SOP vs. Ω_{DS} for various a and b.

10 presents the secrecy outage performance of the considered system with various combinations of channel parameters a and b. The results show that the SOP with a small a outperforms that with a large a, because a large a implies more information being overheard by the eavesdropper. However, the secrecy outage lines for different b, namely, $b = 1$ and 2, overlap with each other, indicating that the eavesdropping link's scale parameter does not influence the secrecy outage performance over the uplink of the considered system.

In Figs. 11, the SOP lines for various R_D fully overlap with each other, which means that adjusting R_D cannot improve or degrade the SOP of the considered system. It can be explained by fact that adjusting R_D will influence the received SNR at both S and E, and then the secrecy outage performance will not change anymore.

Furthermore, it can be seen from Figs. 9 and 10, the derived asymptotic SOP can perfectly match the simulation and analysis ones in the high Ω_{DS} region, which suggests that the proposed asymptotic SOP can be used in practical applications instead of simulation and analysis expressions by exploiting its accuracy in high Ω_{DS} region.

Finally, as presented in Figs. 5 - 11, it is noted that Ω_{SD} and Ω_{DS} exhibit the same positive effect on the secrecy outage performance of the considered system. This comes to the fact that a large Ω_{SD}/Ω_{DS} represents a high channel gain for the main link between S and D. Also, simulation and analysis results match very well with each other, which verifies the correctness of our proposed analytical model.

VI. Conclusion

In this work, the secrecy outage performance of the UAV-2-V system has been investigated by deriving the approximated/exact closed-form analytical expressions for the SOP as well as the asymptotic results of both downlink and uplink. We consider the randomness of the positions of UAV, the legitimate vehicle, and the eavesdropping vehicle to make our system more realistic and reasonable.

Observing from the simulation results, we can reach some useful remarks as follows:

1) The maximum and minimum heights that S can reach show a weak influence on the secrecy outage performance over the downlink, while it does not exhibit an obvious impact on the secrecy outage performance over the uplink.

2) The transmit SNR at S provides a weak impact on the SOP over the downlink, while the transmit SNR at D does not show an apparent impact on the SOP over the uplink.

3) The radius of S's ground coverage area exhibits a negative effect on the secrecy outage performance, while the radius of D also does not exhibit an obvious influence on the secrecy outage performance.

VII. Appendix: The Proof of Theorem 1

Firstly, using (3)-(5), we can obtain the joint PDF of (h, p, t, w) as

$$f_{h,p,w,t}(h,p,w,t) = \frac{\mathbb{I}(\text{con})}{R_S(H_{\max}-H_{\min})(R_S^2-p^2)}, \quad (45)$$

where con $= (H_{\min} \leqslant h \leqslant H_{\max}, 0 \leqslant p \leqslant R_S, 0 \leqslant w \leqslant \sqrt{R_S^2-p^2}, 0 \leqslant t \leqslant \sqrt{R_S^2-p^2})$. $\mathbb{I}(\cdot)$ is the indicator function, i.e., $\mathbb{I}(\text{con}) = 1$ when con is true, or $\mathbb{I}(\text{con}) = 0$ when con is false. Then the joint PDF of (h, p, w, y) is given as

$$f_{h,p,w,y}(h,p,w,y) = f_{h,p,w,t}(h,p,w,g(h,p,w,y))|det(J)|, \quad (46)$$

where $g(h,p,w,y) = \sqrt{\frac{1}{y}\left(h^2+p^2+w^2\right) - \left(h^2+p^2\right)}$ and the matrix J is the Jacobian matrix defined as

$$J = \begin{bmatrix} 1 & 0 & 0 & 0 \\ 0 & 1 & 0 & 0 \\ 0 & 0 & 1 & 0 \\ \frac{\partial g(h,p,w,y)}{\partial h} & \frac{\partial g(h,p,w,y)}{\partial p} & \frac{\partial g(h,p,w,y)}{\partial w} & \frac{\partial g(h,p,w,y)}{\partial y} \end{bmatrix}.$$

Substituting J into (46), one can get $f_{h,p,w,y}(h,p,w,y)$ as

$$\begin{aligned} & f_{h,p,w,y}(h,p,w,y) \\ &= \frac{1}{R_S\left(H_{\max}-H_{\min}\right)} \frac{h^2+p^2+w^2}{2y^2 g(h,p,w,y)\left(R_S^2-p^2\right)} \\ &\quad \times \mathbb{I}\Bigg(H_{\min} \leqslant h \leqslant H_{\max}, 0 \leqslant p \leqslant R_S, 0 \leqslant w \\ &\quad \leqslant \sqrt{R_S^2-p^2}, 0 \leqslant g(h,p,w,y) \leqslant \sqrt{R_S^2-p^2} \Bigg). \end{aligned} \tag{47}$$

Then, the PDF of Y is

$$f_Y(y) = \int\int\int f_{h,p,w,y}(h,p,w,y) dh dp dw. \tag{48}$$

In the following, let $a_1 = h^2+p^2$, $b_1 = R_S^2 - p^2$, $c_1 = R_S^2 + h^2$, and $\phi_2 = \frac{{H_{\max}}^2}{{H_{\max}}^2+R_S^2}$, and recall $\phi_1 = \frac{{H_{\min}}^2}{{H_{\min}}^2+R_S^2}$ to simplify the analysis.

To deal with the condition in the indicator function of (47), we first consider $y < 1$. Now we discuss the following two cases:

Case 1: $\phi_1 \leq y < \phi_2$. Thus, the indicator function of (47) can be derived as

$$\begin{aligned} \mathbb{I}\Bigg(& H_{\min} \leqslant h \leqslant \sqrt{\frac{y}{1-y}} R_S,\ 0 \leqslant p \leqslant \sqrt{y(R_S^2+h^2)-h^2}, \\ & 0 \leqslant w \leqslant \sqrt{y(R_S^2+h^2)-h^2-p^2} \Bigg). \end{aligned} \tag{49}$$

Plugging (47) into (48), we obtain that

$$\begin{aligned} & f_Y(y) \\ &= \int_{H\min}^{\sqrt{\frac{y}{1-y}} R_S} \int_0^{\sqrt{y(R_S^2+h^2)-h^2}} \int_0^{\sqrt{y(R_S^2+h^2)-h^2-p^2}} \\ &\quad \frac{1}{R_S(H_{\max}-H_{\min})} \frac{h^2+p^2+w^2}{2y^2 g(h,p,w,y)\left(R_S^2-p^2\right)} dw dp dh \\ &= \frac{1}{\Xi y^{1.5}} \int_{H_{\min}}^{\sqrt{\frac{y}{1-y}} R_S} \int_0^{\sqrt{c_1 y - h^2}} g_1(p,h,y)\, dp dh, \end{aligned} \tag{50}$$

where $g_1(p,h,y) = \frac{a_1(y+1)}{b_1} \log \frac{\sqrt{b_1 y}+\sqrt{c_1 y - a_1}}{\sqrt{a_1(1-y)}} + \sqrt{\frac{c_1 y^2 - a_1 y}{b_1}}$ and $\Xi = 4R_S\left(H_{\max}-H_{\min}\right)$.

Case 2: $\phi_2 \leq y < 1$. Then, the indicator function of (47) can be derived as $\mathbb{I}\Big(H_{\min} \leqslant h \leqslant H_{\max}, 0 \leqslant p \leqslant \sqrt{y(R_S^2+h^2)-h^2}, 0 \leqslant w \leqslant \sqrt{y(R_S^2+h^2)-h^2-p^2}\Big)$.

Similarly, it gives

$$f_Y(y) = \frac{1}{\Xi y^{1.5}} \int_{H_{\min}}^{H_{\max}} \int_0^{\sqrt{c_1 y - h^2}} g_1(p,h,y)\, dp dh. \tag{51}$$

Notice that $Y = \frac{h^2+p^2+t^2}{h^2+p^2+w^2}$ and $1/Y$ are identically distributed, thus we can easily derive that the PDF of Y satisfies $f_Y(y) = \frac{1}{y^2} f_Y\left(\frac{1}{y}\right)$.

Therefore, one can derive that, when $y > 1$, the PDF of $Y = \frac{h^2+p^2+t^2}{h^2+p^2+w^2}$ is

$$f_Y(y) = \begin{cases} \frac{1}{\Xi y^{1.5}} \int_{H_{\min}}^{H_{\max}} \int_0^{\sqrt{\frac{c_1}{y}-h^2}} g_2(p,h,y)\, dp dh, & 1 < y \leqslant \frac{1}{\phi_2} \\ \frac{1}{\Xi y^{1.5}} \int_{H_{\min}}^{\sqrt{\frac{R_S^2}{y-1}}} \int_0^{\sqrt{\frac{c_1}{y}-h^2}} g_2(p,h,y)\, dp dh, & \frac{1}{\phi_2} < y \leqslant \frac{1}{\phi_1} \end{cases}, \tag{52}$$

where $g_2(p,h,y) = \frac{a_1(y+1)}{b_1} \log \frac{\sqrt{b_1}+\sqrt{c_1 - a_1 y}}{\sqrt{a_1(y-1)}} + \sqrt{\frac{c_1 - a_1 y}{b_1}}$.

Thus, combining (50), (51), and (52) completes the proof.

REFERENCES

[1] M. Mozaffari, W. Saad, M. Bennis, and M. Debbah, "Mobile unmanned aerial vehicles (UAVs) for energy-efficient Internet of things communications," *IEEE Trans. Wireless Commun.*, vol. 16, no. 11, pp. 7574-7589, Nov. 2017.

[2] M. Mozaffari, W. Saad, M. Bennis, Y.-H. Nam, and M. Debbah, "A tutorial on UAVS for wireless networks: Applications, challenges, and open problems," *IEEE Commun. Surveys Tuts.*, vol. 21, no. 3, pp. 2334-2360, 3rd Quart. 2019.

[3] A. Fotouhi, H. Qiang, M. Ding, M. Hassan, L. G. Giordano, A. Garcia-Rodriguez, and J. Yuan, "Survey on UAV cellular communications: Practical aspects, standardization advancements, regulation, and security challenges," *IEEE Commun. Surveys Tuts.*, vol. 21, no. 4, pp. 3417-3442, 4th Quar. 2019.

[4] R. Fan, J. Cui, S. Jin, K. Yang, and J. An, "Optimal node placement and resource allocation for UAV relaying network," *IEEE Commun. Lett.*, vol. 22, no. 4, pp. 808-811, Feb. 2018.

[5] Y. Chen, W. Feng, and G. Zheng, "Optimum placement of UAV as relays," *IEEE Commun. Lett.*, vol. 22, no. 2, pp. 248-251, Feb. 2018.

[6] G. Pan, J. Ye, Y. Zhang, and M.-S. Alouini, "Performance analysis and optimization of cooperative satellite-aerial-terrestrial systems," *IEEE Trans. Wireless Commun.*, vol. 19, no. 10, pp. 6993-6707, Oct. 2020.

[7] S. Chandrasekharan, K. Gomez, A. Al-Hourani, S. Kandeepan, T. Rasheed, L. Goratti, L. Reynaud, D. Grace, I. Bucaille, T. Wirth, and S. Allsopp, "Designing and implementing future aerial communication networks," *IEEE Commun. Mag.*, vol. 54, no. 5, pp. 26-34, May 2016.

[8] M. Alzenad, A. El-Keyi, F. Lagum, and H. Yanikomeroglu, "3-D placement of an unmanned aerial vehicle base station (UAV-BS) for energy-efficient maximal coverage," *IEEE Wireless Commun. Lett.*, vol. 6, no. 4, pp. 434-437, Aug. 2017.

[9] D. Wang, B. Bai, G. Zhang, and Z. Han, "Optimal placement of low-altitude aerial base station for securing communications," *IEEE Wireless Commun. Lett.*, vol. 8, no. 3, pp. 869-872, Jun. 2019.

[10] G. Pan, H. Lei, J. An, S. Zhang, and M.-S. Alouini, "On the secrecy of UAV systems with linear trajectory," *IEEE Trans. Wireless Commun.*, vol. 19, no. 10, pp. 6277-6288, Oct. 2020.

[11] J. Ye, C. Zhang, H. Lei, G. Pan, and Z. Ding, "Secure UAV-to-UAV systems with spatially random UAVs," *IEEE Wireless Commun. Lett.*, vol. 8, no. 2, pp. 564-567, Apr. 2019.

[12] A. A. Khuwaja, Y. Chen, N. Zhao, M. Alouini, and P. Dobbins, "A survey of channel modeling for UAV communications," *IEEE Commun. Surveys Tuts.*, vol. 20, no. 4, pp. 2804-2821, 4th Quart. 2018.

[13] S. Enayati, H. Saeedi, H. Pishro-Nik, and H. Yanikomeroglu, "Moving aerial base station networks: A stochastic geometry analysis and design perspective," *IEEE Trans. Wireless Commun.*, vol. 18, no. 6, pp. 2977-2988, Jun. 2019.

[14] P. K. Sharma and D. I. Kim, "Random 3D mobile UAV networks: Mobility modeling and coverage probability," *IEEE Trans. Wireless Commun.*, vol. 18, no. 5, pp. 2527-2538, May 2019.

[15] M. Bloch and J. Barros, *Physical-Layer Security: From Information Theory to Security Engineering*. Cambridge: Cambridge University Press, 2011.

[16] Z. Xiang, W. Yang, G. Pan, Y. Cai, Y. Song, and Y. Zou, "Secure transmission in HARQ-assisted non-orthogonal multiple access networks," *IEEE Trans. Inf. Forensics Security*, vol. 15, pp. 2171-2182, Jan. 2020.

[17] G. Pan, J. Ye, C. Zhang, J. An, H. Lei, Z. Ding, and M. S. Alouini, "Secure cooperative hybrid VLC-RF systems," *IEEE Trans. Wireless Commun.*, vol. 19, no. 11, pp. 7097-7107, Nov. 2020.

[18] J. Yao, S. Feng, X. Zhou, and Y. Liu, "Secure routing in multihop wireless ad-hoc networks with decode-and-forward relaying," *IEEE Trans. Commun.*, vol. 64, no. 2, pp. 753-764, Feb. 2016.

[19] T. Bao, H.-C. Yang, and M. O. Hasna, "Secrecy performance analysis of UAV-assisted relaying communication systems," *IEEE Trans. Veh. Technol.*, vol. 69, no. 1, pp. 1122-1126, Jan. 2020.

[20] B. Ji, Y. Li, D. Cao, C. Li, S. Mumtaz, and D. Wang, "Secrecy performance analysis of UAV assisted relay transmission for cognitive network with energy harvesting," *IEEE Trans. Veh. Technol.*, vol. 69, no. 7, pp. 7404-7415, Jul. 2020.

[21] T. Bao, J. Zhu, H.-C. Yang, and M. O. Hasna, "Secrecy outage performance of ground-to-air communications with multiple aerial eavesdroppers and its deep learning evaluation," *IEEE Wireless Commun. Lett.*, vol. 9, no. 9, pp. 1351-1355, Sept. 2020.

[22] J. Tang, G. Chen, and J. P. Coon, "Secrecy performance analysis of wireless communications in the presence of UAV jammer and randomly located UAV eavesdroppers," *IEEE Trans. Inf. Forensics Security*, vol. 14, no. 11, pp. 3026-3041, Nov. 2019.

[23] X. Zhou, Q. Wu, S. Yan, F. Shu, and J. Li, "UAV-enabled secure communications: Joint trajectory and transmit power optimization," *IEEE Trans. Veh. Technol.*, vol. 68, no. 4, pp. 4069-4073, Apr. 2019.

[24] P. K. Sharma and D. I. Kim, "Secure 3D mobile UAV relaying for hybrid satellite-terrestrial networks," *IEEE Trans. Wireless Commun.*, vol. 19, no. 4, pp. 2770-2784, Apr. 2020.

[25] Q. Yuan, Y. Hu, C. Wang, and Y. Li, "Joint 3D beamforming and trajectory design for UAV-enabled mobile relaying system," *IEEE Access*, vol. 7, pp. 26488-26496, Mar. 2019.

[26] C. Zhong, J. Yao, and J. Xu, "Secure UAV communication with cooperative jamming and trajectory control," *IEEE Commun. Lett.*, vol. 23, no. 2, pp. 286-289, Feb. 2019.

[27] A. A. Khuwaja, Y. Chen, and G. Zheng, "Effect of user mobility and channel fading on the outage performance of UAV communications," *IEEE Wireless Commun. Lett.*, vol. 9, no. 3, pp. 367-370, Mar. 2020.

[28] T. Hou, Y. Liu, Z. Song, X. Sun, and Y. Chen, "Multiple antenna aided NOMA in UAV networks: A stochastic geometry approach," *IEEE Trans. Commun.*, vol. 67, no. 2, pp. 1031-1044, Feb. 2019.

[29] H. Lei, D. Wang, K.-H. Park, I. S. Ansari, J. Jiang, G. Pan, and M.-S. Alouini, "Safeguarding UAV IoT communication systems against randomly located eavesdroppers," *IEEE Internet Things J.*, vol. 7, no. 2, pp. 1230-1244, Feb. 2020.

[30] R. Ma, W. Yang, Y. Zhang, J. Liu, and H. Shi, "Secure mmWave communication using UAV-enabled relay and cooperative jammer," *IEEE Access*, vol. 7, pp. 119729-119741, Sept. 2019.

[31] X. Sun, W. Yang, and Y. Cai, "Secure communication in NOMA assisted millimeter wave SWIPT UAV networks," *IEEE Internet Things J.*, vol. 7, no. 3, pp. 1884-1897, Mar. 2020.

[32] H. Menouar, I. Guvenc, K. Akkaya, A. S. Uluagac, A. Kadri, and A. Tuncer, "UAV-enabled intelligent transportation systems for the smart city: Applications and challenges," *IEEE Commun. Mag.*, vol. 55, no. 3, pp. 22-28, Mar. 2017.

[33] S. A. Hadiwardoyo, J.-M. Dricot, C. T. Calafate, J.-C. Cano, E. Hernandez-Orallo, and P. Manzoni, "UAV mobility model for dynamic UAV-to-car communications," in *Proc. Proceedings of the 16th ACM International Symposium on Performance Evaluation of Wireless Ad Hoc, Sensor, & Ubiquitous Networks*, Miami Beach, FL, USA, Nov. 2019, pp. 1-6.

[34] S. A. Hadiwardoyo, C. T. Calafate, J.-C. Cano, K. Krinkin, D. Klionskiy, E. Hernandez-Orallo, and P. Manzoni, "Optimizing UAV-to-car communications in 3D environments through dynamic UAV positioning," in *Proc. Proceedings of the 23rd IEEE/ACM International Symposium on Distributed Simulation and Real Time Applications*, Cosenza, Italy, Oct. 2019, pp. 67-74.

[35] I. S. Gradshteyn and I. M. Ryzhik, *Table of Integrals, Series and Products*,7th. San Diego, CA, USA: Academic, 2007.

[36] M. Abramowitz and I. Stegun, *Handbook of Mathematical Functions With Formulas, Graphs, and Mathematical Tables*, 9th. New York, NY, USA: Discover, 1972.

[37] I. Sen and D. W. Matolak, "Vehicle-vehicle channel models for the 5-GHz band," *IEEE Trans. Intell. Transp. Syst.*, vol. 9, no. 2, pp. 235-245, Jun. 2008.

[38] H. Lei, Y. Zhang, K.-H. Park, I. S. Ansari, G. Pan, and M.-S. Alouini, "Performance analysis of dual-hop RF-UWOC systems," *IEEE Photon. J.*, vol. 12, no. 2, pp. 1-15, Apr. 2020.

[39] A. P. Prudnikov, Y. A. Brychkov, and O. I. Marichev, *Integrals and Series: Vol. 3: More Special Functions*. New York, NY, USA: Gordon and Breach Science Publishers, 1992.

[40] V. S. Adamchik and O. I. Marichev, "The algorithm for calculating integrals of hypergeometric type functions and its realization in REDUCE system," in *Proc. the international symposium on Symbolic and algebraic computation (ISSAC '90)*, Tokyo, Japan, Aug. 1990, pp. 212-224.

[41] M. Di Renzo, A. Guidotti, and G. E. Corazza, "Average rate of downlink heterogeneous cellular networks over generalized fading channels: A stochastic geometry approach," *IEEE Trans. Commun.*, vol. 61, no. 7, pp. 3050-3071, Jul. 2013.

[42] H. Lei, Z. Yang, K.-H. Park, I. S. Ansari, Y. Guo, G. Pan, and M.-S. Alouini, "Secrecy outage analysis for cooperative NOMA systems with relay selection schemes," *IEEE Trans. Commun.*, vol. 67, no. 9, pp. 6282-6298, Sept. 2019.

[43] E. Zedini and M. S. Alouini, "On the performance of multihop heterodyne FSO systems with pointing errors," *IEEE Photon. J.*, vol. 7, no. 2, pp. 1-10, Apr. 2015.

Tingting Li received her B.Sc in Mathematics and Applied Mathematics in 2006 and the Ph.D. degree in Computational Mathematics in 2012 from Chongqing University, Chongqing, China. In July 2012, She joined the School of Mathematics and Statistics, Southwest University, Chongqing, China where she is currently an Associate Professor. Her research interests include statistics and its applications.

Jia Ye (Student Member, IEEE) received the B.Sc. degree in communication engineering from Southwest University, Chongqing, China, in 2018, and received the M.S. degree from King Abdullah University of Science and Technology (KAUST), Saudi Arabia, in 2020. Now, she is a PhD student at King Abdullah University of Science and Technology (KAUST), Saudi Arabia. Her main research interests include the performance analysis and modeling of wireless communication systems.

Jibo Dai received the B.S. degree and the M.S. degree in information and communication engineering from Beijing Institute of Technology, China, in 2014 and 2017, respectively. He is currently an engineer with National Key Laboratory of science and Technology on Aerospace Intelligence Control, China, and he is also with Beijing Aerospace Automatic Control Institute, China. His research interests include data link system design, integrated electronics system design, wireless Ad-hoc network, data link system and network for UAV swarm, etc.

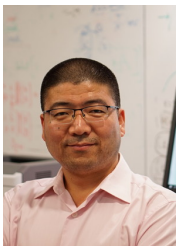

Hongjiang Lei (Senior Member, IEEE) received the B.Sc. degree in Mechanical and Electrical Engineering from Shenyang Institute of Aeronautical Engineering, Shenyang, China, in 1998, the M.Sc. degree in Computer Application Technology from Southwest Jiaotong University, Chengdu, China, in 2004, and the Ph.D. degree in Instrument Science and Technology from Chongqing University, Chongqing, China, in 2015, respectively. In May 2004, he joined the School of Communication and Information Engineering (SCIE) of Chongqing University of Posts and Telecommunications (CQUPT), Chongqing, China, where he is currently a full professor. From November 2016 to October 2018, he was a Postdoctoral Research Fellow with CEMSE Division, King Abdullah University of Science and Technology (KAUST), Saudi Arabia. His current research interests include physical layer security, cooperative relaying systems, and cognitive radio networks.

Weiwei Yang received the B.S., M.S., and Ph.D. degrees from the College of Communications Engineering, PLA University of Science and Technology, Nanjing, China, in 2003, 2006, and 2011, respectively. He is currently an Associate Professor and a Doctoral Supervisor with the Institution of Communications Engineering, Army Engineering University of PLA. His research interests include cooperative communications, cognitive radio, covert communications, and physical layer security.

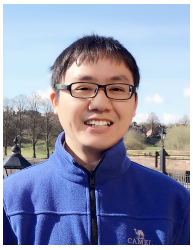

Gaofeng Pan (Senior Member, IEEE) received his B.Sc in Communication Engineering from Zhengzhou University, Zhengzhou, China, in 2005, and the Ph.D. degree in Communication and Information Systems from Southwest Jiaotong University, Chengdu, China, in 2011. He is with the School of Cyberspace Science and Technology, Beijing Institute of Technology, P. R. China, as a professor. His research interest spans special topics in communications theory, signal processing, and protocol design.

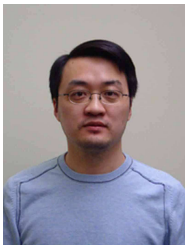

Yunfei Chen (Senior Member, IEEE) received his B.E. and M.E. degrees in electronics engineering from Shanghai Jiaotong University, Shanghai, P.R.China, in 1998 and 2001, respectively. He received his Ph.D. degree from the University of Alberta in 2006. He is currently working as an Associate Professor at the University of Warwick, U.K. His research interests include wireless communications, cognitive radios, channel modeling, SNR estimation, diversity, modulation and UWB systems.